RSC Advances

PAPER

View Article Online
View Journal | View Issue

Cite this: *RSC Adv.*, 2023, **13**, 2123

The impact of silver nanoclay functionalisation on optical and electrochemical properties

Sapokazi Timakwe, Bongiwe Silwana and Mangaka C. Matoetoe *

Three different fractions of nanoclay (nanomer 1.44P) were functionalised with Ag forming silver nanoclay composites (Ag/nanomer 1.44P). The optical and electrochemical properties of the functionalised nanoclay were studied. Optical, morphology, and electrochemical techniques were used for the characterisation of the synthesised Ag/nanomer 1.44P nanocly composites. The presence and the absence of functional groups observed in the FTIR spectrum of Ag/nanomer 1.44P, compared with those found in the spectra of silver and pure nanomer 1.44P prove that a reaction occurred, thus a successful functionalisation of nanomer 1.44P nanoclay with silver. The XRD data of all composites showed four diffraction peaks within the silver spectrum range, with the intensity of silver decreasing with increasing concentration of nanomer 1.44P. SEM represented well-dispersed particles of different shapes with average particle sizes of 2.5, 27.5, and 5 nm with the enhanced concentration of nanomer 1.44P nanoclay. The decrease in diffusion coefficient values from 4.26×10^{-10}, 2.50×10^{-13} , 1.40×10^{-13} $cm^2\ s^{-1}$ and electron transfer rates of 1.50×10^{-5}, 3.94×10^{-7}, 2.86×10^{-7} $cm\ s^{-1}$ are respectively proportional to an increase in nanomer 1.44P concentration depicting changes in nanocomposites sizes.

Received 17th October 2022
Accepted 24th November 2022

DOI: 10.1039/d2ra06549e

rsc.li/rsc-advances

1 Introduction

Nanoclays as nanofillers are incorporated in nanotechnology studies to enhance the quality of the material due to their inexpensiveness, mineral-rich content, ever-availability, high surface area, increased stability, resistance to extreme temperatures, excellent intercalation properties and environmental amiability.[1–3] They are phyllosilicates dominant, made of SiO_4 tetrahedra polymeric layers attached to (Mg, Fe, Al) $(O, OH)_6$ octahedra thin sheets.[3] Over four thousand clay minerals have been discovered including montmorillonite, zeolites, and sepiolite being the most popular clay minerals.[3] However, montmorillonite clay has been extensively used in the production of hybrids and composites because its layered structure is joined together by weak van der Waals and electrostatic forces, making it easy to modify.[4,5] The interlayer space of montmorillonite clay act as the adsorbent for cationic ions, and as a support for binding transition metal complex catalysts in the synthesis of material and biomaterial nanoparticles.[6] Clay-modified electrodes provide high chemical stability, good biocompatibility, increased analyte mobility, good ion exchange, swelling and adsorption capacity, and increased product mobility.[3,4] The particles of clay have activated sites for assembling electrochemical species but only a few possess redox properties. In the process of nanoclay functionalisation, a species can be adsorbed on the clay in various sites, including an attachment on edges, interlamellar spaces, interparticle spaces, and attachment on the surface.[3] The electrochemical properties of the nanoparticles could be improved by metal nanoparticles decorated with organic or inorganic nanocomposites, exhibiting interactive effects toward target analysis.[7,8] Hence, silver nanoparticles are used to functionalise nanoclays, forming nanocomposites with nanoscale properties that enhance the material's macroscopic quality.[2,9] Silver nanoparticles (AgNPs) are the most important and fascinating materials among several metallic nanoparticles that are involved in biomedical applications. The use of clays is well known to support AgNPs to amplify the electrochemical signal of the bare nanoparticles, which is an important property to produce sensors for different applications. Moreover, silver has been selected due to its antimicrobial activity, rapid charge and mass transport, cost-effectiveness with high specific surface area, and good electrical conductivity compared to other metals.[4,7]

Nanocomposites can be classified as ceramic, metallic, and polymer-based nanocomposites, according to their matrix and structural differences.[3,9] Furthermore, polymers that have good physical and chemical properties are the most applied nanocomposites, which could be due to the shape, size, concentration, and interaction of the incorporated nanoparticles with the polymer matrix.[10] Methods such as extrusion, *in situ*, melt-intercalation, direct mixing, and casting have been implemented in the production of nanocomposites.[2] Others include rapid solidification process, microwave synthesis, complex

Cape Peninsula University of Technology, Chemistry Department, P.O. Box 1906, Symphony Way, Bellville, 7535, South Africa. E-mail: MatoetoeM@cput.ac.za

polymerized, chemical vapour deposition, hydrothermal, template, sol–gel, and high-energy ball milling processes.

Various methods including optical, morphology, and electrochemical techniques were used to characterise silver nanoclay composites prepared using different nanoclays to define the properties of the material. However, there has been no information reported on the synthesis and electrochemical properties of nanomer 1.44P nanoclay with silver. In these regards, the objectives of this study were to prepare Ag-based films reinforced with nanomer 1.44P nanoclay, aiming to improve their optical and electrochemical properties. We compared the fractions and evaluated the microstructure of the different composite films prepared using SEM, FTIR spectroscopy, XRD, CV as well as DPV to define the material's properties, foreseeing their potential applications for future electrochemical applications. Based on the results obtained, the electrochemical properties showed vital aspects of the structural activity.

2 Experimental

2.1 Reagents

Silver nitrate ($AgNO_3$), trisodium citrate dihydrate (TSC), $Na_3C_6H_5O_7 \cdot 2H_2O$, hydrochloric acid (HCl), and nanomer 1,44P nanoclay were purchased from Sigma-Aldrich, UK and used without purifying further. Milli-Q water from the Millipore system was used throughout the experiment.

2.2 Synthesis of silver nanomer 1.44P nanoclay composites

Novel silver nanomer 1.44P nanoclay composite was synthesised by dissolving 0.0169 g of $AgNO_3$ in 100 ml Milli-Q water. Different masses (0.5 g, 1 g, and 1.5 g) of nanomer 1.44P nanoclay were mixed with 60 mL of 1.0 mM silver nitrate solution separately. The mixtures were covered and heated to boiling while stirring for 20 minutes at 240 °C, 265 rpm, followed by the dropwise addition of 4 mL, 0.1 M solutions of trisodium citrate dihydrate. The mixtures were heated for another 15 minutes and cooled to room temperature. The products were cleaned several times with Milli-Q water through centrifugation.

2.3 The electrode surface modification with silver nanomer 1.44P nanoclay composite

In the modification process, the cleaning of the working electrode was performed with alumina slurry of particle sizes 1.0, 0.3, and 0.05 μm on a polishing pad, followed by 5 min of sonication of GCE in water and ethanol between the polishing steps. A drop-and-dry method was used for the modification of the surface of the glassy carbon electrode (GCE). About 5 μL of nanomer 1.44P nanoclay silver composites was drop-coated on the GCE electrode surface and dried in an open vacuum for 26 minutes before the measurements. Electrochemical measurements were achieved in a 3 mL solution of 0.1 M HCl supporting electrolyte, which was degassed for one minute before measuring.

2.4 Characterization techniques

FTIR was used to characterise functional groups of AgNPs, nanomer 1.44P nanoclay, and the composite at different nanoclay masses. FTIR characterisation was performed using a PerkinElmer spectrometer (USA) between the wavenumber 3700 cm^{-1} and 700 cm^{-1}. The sample holder and the presser were cleaned with acetone and the background noise was measured to eliminate interfering substances. The samples, depending on their nature (solid or liquid) were scanned by compressing them onto the sample holder and the spectra were recorded. XRD patterns were recorded using a multipurpose X-ray diffractometer D8-Advance from BRUKER AXS (Germany) operated under a continuous scan in a locked coupled mode with Cu Kα radiation. The samples were mounted in the centre of the sample holder on a glass slide and levelled up to the correct height. The measurements scanned within a range of 2-theta, with a typical step size of 0.034° in 2. A position-sensitive detector, Lyn-Eye, was used to record the diffraction data at a typical speed of 0.5 s per step, which is equivalent to an effective time of 92 s per step for a scintillation counter. SEM images were taken with the Tescan MiraGMU SEM (Czech Republic) and analysed using imageJ, a java-based image processing program. The size distribution was investigated statistically by measuring the diameter of random nanoparticles. Autolab PGSTAT 101 (Metrohm, South Africa) was used for electrochemical measurements using the software NOVA 2.1. The measurements were carried out at room temperature (25 °C) using a three-electrode system that consists of a glassy carbon electrode (GCE) as a working electrode ($A = 0.071$ cm^2), platinum wire (3 mm diameter) as a counter electrode and Ag/AgCl (3 M KCl) as the reference electrode.

3 Results and discussion

3.1 FTIR characterisation of silver nanoclay composites

FT-IR analysis was carried out to identify the possible interaction of silver nanoparticles with nanomer 1.44P at different masses, as shown in Fig. 1 and Table 1. Comparing the spectra of pure nanomer 1.44P, AgNPs, and different fractions of Ag/nanomer 144P nanoclay (0.5 g, 1 g, and 1.5 g) some peaks of nanomer 1.44P nanoclay, at frequencies 915, 1006, 1472 cm^{-1} and 2931 were not present in FTIR spectra of AgNPs and nanocomposite. The peaks can be ascribed to the presence of Al–OH, SiO stretching, CN, and C–H stretching vibration of the $-CH_2$ group from the aliphatic chains, respectively. Observations in the spectra of the nanocomposite proved the interaction occurring as a shift in the O–H groups of the pure nanomer 1.44P nanoclay was observed. The carbonyl and carboxylic functional groups may be due to the citrate capping agent that reduced Ag ions within clay composites.

Comparing the spectra of pure nanomer 1.44P, AgNPs, and different fractions of Ag/nanomer 144P nanoclay (0.5 g, 1 g, and 1.5 g) some of the peaks of nanomer 1.44P nanoclay at frequencies 915, 1006, 1472 cm^{-1} and 2931 were not present in the FTIR spectra of AgNPs and nanocomposite. The peaks can be ascribed to the presence of Al_2 OH, SiO stretching, CN, and

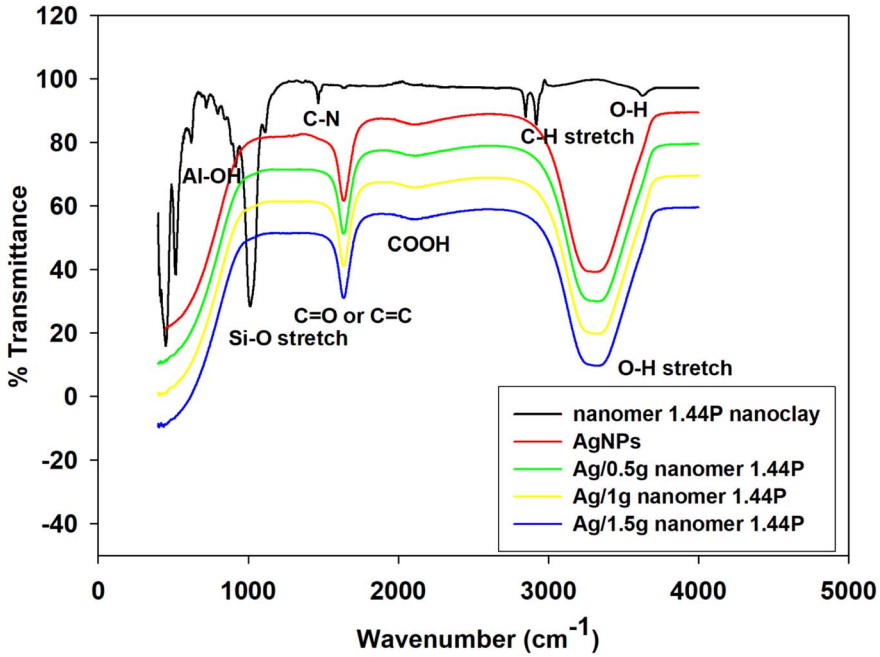

Fig. 1 Overlayed FTIR spectra of 1.44P nanoclay, AgNPs, and different fractions of the Ag/1.44P composites.

Table 1 Comparison of FTIR bands of AgNPs, pure nanomer 1.44P nanoclay and nanomer 1.44P nanoclay nanocomposite at different fractions (0.5 g, 1 g, and 1.5 g)

Functional groups					
Material	AgNPs	Pure 1.44P Clay	0.5 g	1 g	1.5 g
Al–OH	—	915	—	—	—
Si–O stretch	—	1006	—	—	—
C–N	—	1472	—	—	—
C–H stretch	—	2844–2931	—	—	—
O–H	3288	3648	3306	3307	3302
C=O or C=C	1626	—	1629	1648	1645
COOH	2107	—	2124	2124	2126

C–H stretching vibrations of the $-CH_2$ group from the aliphatic chains, respectively. Observations in the spectra of nanocomposite prove that there was an interaction that occurred as can be seen by a shift in the O–H group of the pure nanomer 1.44P nanoclay. The carbonyl and carboxylic functional groups may be due to the citrate capping agent, which caused the reduction of Ag ions within the clay composites.

The interaction could be due to the silicate layers of nanomer 1.44P nanoclay and silver nanoparticles, as a result of the presence of van der Waals interactions with the O–H group of 1.44P nanoclay and the partial positive charge on the silver nanoparticle surface.[6]

Moreover, the O–H molecule involves hydrogen bonding between different molecules having instantaneous arrangements, hence, the broad O–H stretching absorption beyond 3000 cm^{-1}. The C=O intense infra-red stretching absorptions observed around 1600 cm^{-1} in Ag/1.44P is due to the large dipole moment.[11] These FTIR results are a proof of the successful functionalization of nanoclays with silver and the summary of the shift in the frequencies is tabulated in Table 1.

3.2 X-ray diffraction characterisation of silver nanoclay composites

The XRD patterns of silver nanoparticles and silver nanoclay composites in the 2θ range of 20° to 80° are shown in Fig. 2.

Silver nanoparticle XRD patterns show four diffraction peaks at 38°, 44°, 64°, and 78°, which corresponds with 111, 200, 220, and 311, as observed in Fig. 2(a), which is in agreement with the literature.[12,13] In the case of the XRD patterns of the silver

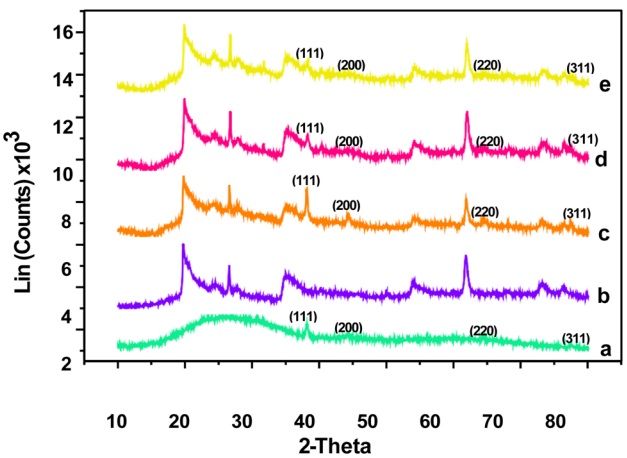

Fig. 2 Overlayed XRD patterns of AgNPs (a), nanomer 1.44P nanoclay (b), and Ag/nanomer 144P nanoclay composites at different fractions 0.5 (c), 1 (d), and 1.5 g nanomer 1.44P nanoclay (e).

nanoclay composites, the same diffraction peaks, which are associated with silver as supported by the literature,[12] were observed, and the intensity of the peaks decreased with enhanced nanoclay concentration from 0.5 g, 1 g, and 1.5 g.

1.44P, the Ag/0.5 g 1.44P composite showed the increased intensity of diffraction patterns, which suggested smaller-sized crystals.[14] There were other diffraction peaks observed at 22°, 24°, and 26°, which seem to be stable with improved nanoclay concentration. However, diffraction peaks were observed at 32° and 50°, and also at 36°, 55°, 62°, and 74°, which may be due to the increased nanoclay concentration. All these served as proof that there was an interaction between nanoclay and AgNPs, thus confirming the successful functionalisation of nanoclay.

3.3 Scanning electron microscopy of silver nanoclay composites

The SEM images of AgNPs and Ag/1.44P composites formed by changing nanoclay concentrations are shown in Fig. 3.

The SEM images of AgNPs show particle size with an average diameter of 17.5 nm. However, there is some evidence of aggregation, where smaller nanoparticles merge with each other, resulting in bigger-sized AgNPs that are less distributed, forming clusters and bunches that do not cover the entire surface of the holder.[15] This might be due to a decrease in the interaction of nanoparticles. The effect of functionalising nanoclay with AgNPs led to the formation of silver nanoclay composites of different particle sizes and shapes. However, Ag/1 g 1.44P composites show particles with an average size of 27.5 nm, which is greater than that of AgNPs. From the SEM images in Fig. 3, the sizes for Ag/1 g and Ag/1.5 g 1.44P seem small and well-dispersed as a result of a decrease in the concentration of silver with increased nanoclay concentration, resulting in more distribution and good coverage on the sample holder. The same trend was observed in the XRD patterns discussed previously, where the intensity of silver was reduced with increasing nanoclay concentrations. Moreover, SEM supported the XRD results wherein the intensity of Ag/0.5 g 1.44P was greater, suggesting that the smaller nanoparticle size with good sensitivity was comparable to other composites. Nanoparticles of smaller size, 2.5 nm, of Ag/0.5 g 1.44P and 5 nm for Ag/1.5 g 144P composites suggested good sensitivity compared to Ag/1 g 1.44P.

3.4 Electrochemical analysis of Ag/1.44P

The cyclic voltammetry (CV) and differential pulse voltammetry (DPV) of silver-functionalised nanoclay composites (Ag/1.44P) were recorded and are represented in Fig. 4 and compared with that of AgNP, as shown in Fig. 4(A).

Based on the representation in Fig. 4(A), the effect of silver on the nanoclay can be observed where the silver signal is present in Ag/1.44P composites within the potential range of silver, which cannot be observed in pure 1.44P voltammogram. Therefore, the conductivity of nanoclay was enhanced by the presence of silver;[2] hence, the peak was observed in silver nanoclay composites.

In reference to Table 2, the difference between the two peak potentials (ΔE_p) revealed information about the reversibility of the species in question and is given by eqn (4.1), with eqn (4.2) used to deduce the number of electrons involved.

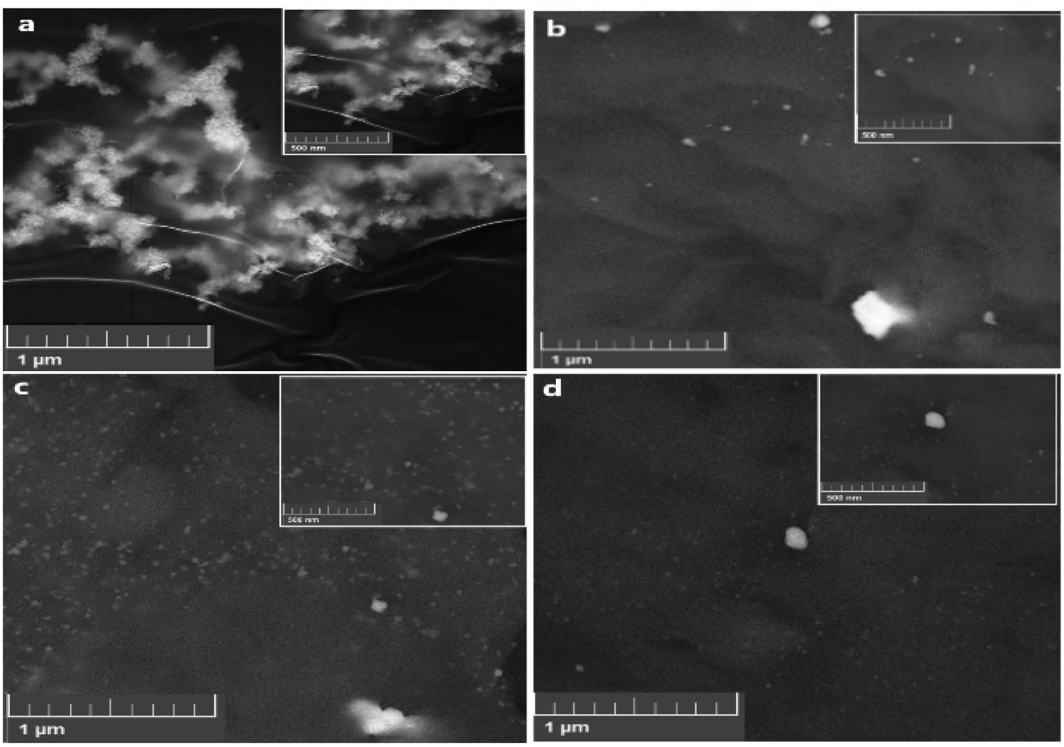

Fig. 3 SEM images of AgNPs (a) Ag/1.44P composites with (b) 0.5 (c) 1 (d) 1.5 g 1.44P. Inset: magnification of the SEM images at 500 μm.

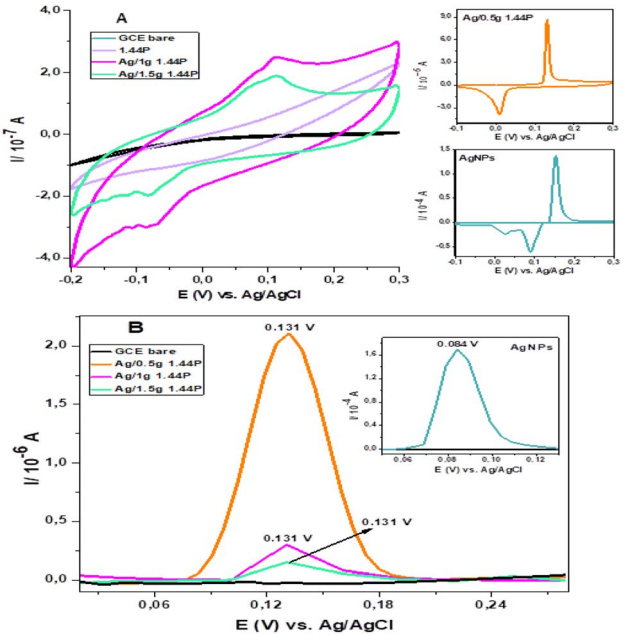

Fig. 4 (A) CV of AgNPs, 1.44P nanoclay, Ag/1.44P composites at 0.08 V s^{-1}. (B) DPV of AgNPs, Ag/1.44P composites at a potential step 8 mV at GCE in 0.1 M HCl.

$$\Delta E_p = \Delta E_{pa} - \Delta E_{pc} = \frac{0.0592}{n} \quad (4.1)$$

$$\left| E_{pa} - \frac{E_{pa}}{2} \right| = 2.20 \frac{RT}{nF} \quad (4.2)$$

where E_{pa} and E_{pc} are anodic and cathodic peak potentials (V), respectively, n is the number of electrons involved, R is the gas constant (J K^{-1} mol^{-1}), T is the absolute temperature (kelvin), and F is the Faraday's constant (C mol^{-1}).

For a reversible electrode reaction, ΔE_p is expected to be 0.0592, whereas enhanced ΔE_p values represent quasi-reversible behaviour.[16] Thus, the obtained values confirm the quasi-reversibility. In comparison with CV for AgNPs, there is a shift in the peak potentials observed cathodically for composites with increased concentration of the nanoclay, as represented in Table 1, with Ag/1 g 1.44P having less positive potential compared to other nanoclay composites, indicating smaller-sized nanoparticles. The smaller-sized particles revealed by CV with less positive potential are due to the decrease in silver nanoparticle concentration, allowing the composites to highly cover the electrode surface. In contrast, Ag/0.5 g 1.44P has a more positive potential due to more silver present that showed aggregation agreeing with SEM results. However, DPV in Fig. 4(B) depicted more positive potentials for Ag/1 g and Ag/1.5 g 1.44P composites. The potential for Ag/0.5 g 1.44P, however, slightly decreased in DPV from that of CV. In addition, the conductivity of nanoclay composites seems to increase with reduced nanoclay concentration because lesser nanoclay concentration implies more silver concentration in the composite solution, hence higher conductivity, which is a good indication.

In the process of synthesizing Ag/1.44P composites, the literature states that the guest cations can be introduced in the interlayer space clay through ion exchange reactions or chemical interactions.[5] As a result of the weak van der Waals force and strong hydration capability of Na^+ ions between the layers of 1.44P nanoclay in the presence of water, the nanoclay swells and exfoliated causing layers to delaminate,[17] as can be seen in the produced Ag/1.44P composites in Fig. 5.

The results show an increase in peak currents, which slide apart as a function of scan rate, depicting a quasi-reversible system.[18,19] The shift in the reduction and oxidation peaks both cathodically and anodically with improved scan rate is an indication of controlled mass transport processes.[20] The electrochemical parameters of the composites, which are related to particle size determination, were calculated using Randles–Sevcik eqn (4.3) to (4.6) and compared with those of silver to confirm the improvement of electrochemical properties of the materials.

Table 2 CV potentials of silver and composites with changes in the concentration of nanoclay using anodic peak data

Material	E_{pa} (V)	E_{pc} (V)	ΔE_p (V)	n	I_{pa} (A) $\times 10^{-7}$	I_{pc} (A) $\times 10^{-7}$
AgNPs	0.151	0.085	0.066	0.75	1340	−557
Ag/0.5 g 1.44P	0.132	0.007	0.125	0.85	87	−37
Ag/1 g 1.44P	0.112	−0.087	0.199	1.00	2.69	−2.99
Ag/1.5 g 1.44P	0.119	−0.073	0.192	0.94	1.84	−2.07

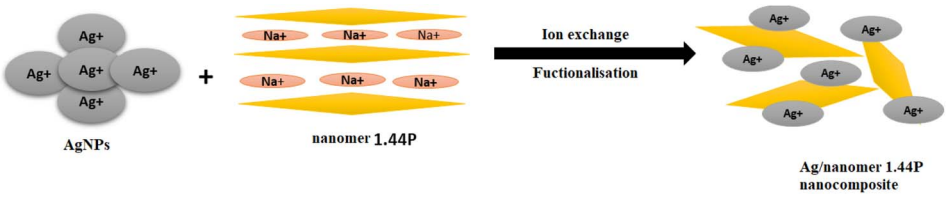

Fig. 5 Functionalisation of nanoclay. The kinetic studies of the synthesised material were investigated with the corresponding voltammograms represented in Fig. 6.

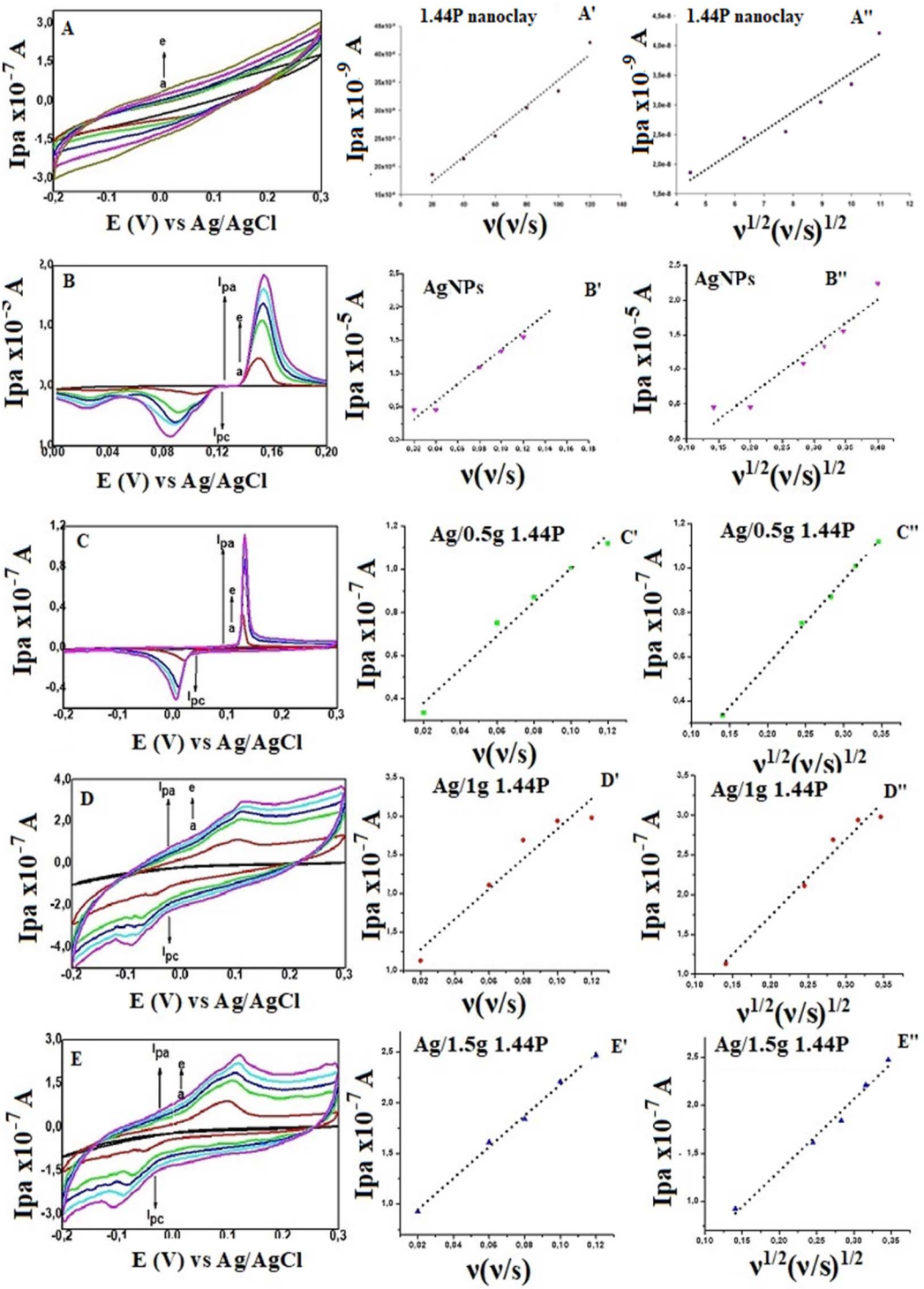

Fig. 6 Overlay of various scan rates studies (A–E) for pure nanomer 1.44P nanoclay, AgNPs, and different fractions of the nanocomposite at scan rates 20–120 V s^{-1}, respectively. Randle's linear dependence plots of the scan rate (A′–E′) and square root scan rate (A″–E″) in the 0.1 M HCl supporting electrolyte.

$$I_p = 2.69 \times 10^5 n^{3/2} A D_0^{1/2} C_{ox} \nu^{1/2} \quad (4.3)$$

$$\text{Slope} = \frac{n^2 F^2 A \Gamma}{4RT} \quad (4.4)$$

$$\Gamma = \frac{Q}{nFA} \quad (4.5)$$

$$K_s = \frac{I_p}{nFAC} \quad (4.6)$$

Table 3 Electrochemical parameters of the modified GCE with AgNPs and Ag/1.44P composites

Material	Slope $\times 10^{-7}$ I_{pa} *vs.* $v^{1/2}$	D ($cm^2\ s^{-1}$) $\times 10^{-13}$	K_s ($cm\ s^{-1}$) $\times 10^{-7}$	Γ ($mol\ cm^{-2}$) $\times 10^{-13}$	Q ($C\ cm^{-2}$) $\times 10^{-10}$
AgNPs	6890	91.20	45 000	184 000	1 044 400
Ag/0.5 g 1.44P	381	4260	150	7940	46 000
Ag/1 g 1.44P	9.63	2.50	3.94	1.45	9.89
Ag/1.5 g 1.44P	7.45	1.40	2.86	1.27	8.14

where I_p is the anodic peak current (A), A is the glassy carbon electrode surface area (0.0707 cm^2), C is the concentration of the electrolyte ($mol\ cm^{-3}$), D is the diffusion current ($cm^2\ s^{-1}$), v is the scan rate ($V\ s^{-1}$). Γ is the surface coverage of the adsorbed species ($mol\ cm^{-2}$), Q is the charge ($C\ cm^{-2}$), K_s is the heterogeneous rate constant ($cm\ s^{-1}$).

Referring to the Randle's plot in Fig. 6A′, B′ and E′, better linearity was observed in peak current *vs.* scan rates for pure nanomer 1.44P, AgNPs, and Ag/1.5 g 1.44P, respectively. This linear relationship was, even more, better in Ag/1.5 g 1.44P, which is attributed to the adsorption-controlled process. However, all plots (Fig. 6C″, D″ and E″) presented a linear tendency for peak current data *vs.* square root of the scan except for pure 1.44P nanomer and AgNPs suggesting diffusion-controlled processes for Ag/0.5 g 1.44P, Ag/1 g 1.44P, and Ag/1.5 g 1.44P. Moreover, the kinetics parameters are revealed in Table 3. As per the results recorded in Table 3, using the slope of the square root scan plot, the behaviour of the material was revealed.

It can be observed that the values of these parameters were high at lower nanoclay concentrations due to more concentration of the silver present, which decreases with increasing concentration of nanoclay leading to lower conductivity, thus smaller values are depicted. The greater values of D and K_s for Ag/0.5 g 1.44P suggests smaller sized nanoparticles, which travel faster leading to increased surface coverage or area compared to larger nanoparticles, which in this case are Ag/1 g 1.44P and Ag/1.5 g 1.44P produced at higher nanoclay mass fractions. Previous studies revealed that the smaller-sized nanoparticles have enhanced D values in comparison with bigger-sized molecules,[19,20] with the arrangement 0.5 > 1 > 1.5 g 1.44P, as shown in Table 3. The literature also states that smaller nanoparticles travel faster in the solution, thus having greater K_s value compared to larger nanoparticles, which travel most slowly in the solution due to the mass, hence smaller K_s value.[21] Moreover, smaller nanoparticles are associated with good sensitivity, hence better charge for Ag/0.5 g 1.44P. However, that was not the case for Ag/1 g and Ag/1.5 g 1.44P due to the improved amount of nanoclay. In comparison with AgNPs alone, the electrochemical parameters decreased with the increase in the concentration of nanoclay, resulting in less conductivity, except for the D value, which seemed to improve in the presence of 0.5 g 1.44P, suggesting a smaller size for Ag/0.5 g 1.44P composites.

4 Conclusions

The optical and electrochemical properties of silver nanoclay composites with different concentrations of nanoclay were successfully studied. The electrochemical studies revealed quasi-reversibility for a one-electron transfer reaction. The nature of the reaction occurring at the electrode surface was confirmed to be a mixture of both adsorption and diffusion-controlled processes. The electrochemical parameters examined indicated 0.5 g as the best concentration of nanoclay for a target application. These findings recommend the usefulness of voltammetry as a complementary method that can be applied as a qualitative guide to identifying the size of composites.

Conflicts of interest

There is no conflict of interest to declare.

Acknowledgements

The authors are extremely thankful for the funding from CPUT and NRF grant (116237) in conducting this study. Data relating to this manuscript can be found from the corresponding author on request.

References

1 R. Feng, Y. Y. Jia, Z. Y. Li, Z. Chang and X. H. Bu, Enhancing the stability and porosity of penetrated metal–organic frameworks through the insertion of coordination sites, *Chem. Sci.*, 2018, **9**(4), 950–955.
2 M. S. Nazir, M. H. Mohamad Kassim, L. Mohapatra, M. A. Gilani, M. R. Raza and K. Majeed, Characteristic Properties of Nanoclays and Characterization of Nanoparticulates and Nanocomposites, *Eng. Mater.*, 2016, 37–55.
3 N. P. Shetti, S. J. Malode, S. D. Bukkitgar, G. B. Bagihalli, R. M. Kulkarni, S. B. Pujari, *et al.*, Electro-oxidation and determination of nimesulide at nanosilica modified sensor, *Mater. Sci. Energy Technol.*, 2019, **2**(3), 396–400.
4 F. A. Batista, S. Q. Nascimento, A. B. Sousa, E. F. R. Júnior, P. I. de Almeida Pereira, V. M. Fontenele, *et al.*, Synthesis, characterization and electrochemical properties of composites synthesized from silver-tannic acid hybrid nanoparticles and different clays, *Appl. Clay Sci.*, 2019, **181**, 105219–105225.
5 C. Zhou, D. Tong and W. Yu, Smectite nanomaterials: preparation, properties, and functional applications, in *Nanomaterials from Clay Minerals: A New Approach to Green Functional Materials*, 2019.

6 K. Shameli, M. B. Ahmad, W. M. Z. W. Yunus, N. A. Ibrahim, Y. Gharayebi and S. Sedaghat, Synthesis of silver/montmorillonite nanocomposites using γ-irradiation, *Int. J. Nanomed.*, 2010, **5**(1), 1067–1077.

7 E. Ahmadi, M. R. Eyvani, V. Riahifar, H. Momeneh and C. Karami, Amperometric determination of nevirapine by GCE modified with c-MWCNTs and synthesized 11-mercaptoundecanoyl hydrazinecarbothioamide coated silver nanoparticles, *Microchem. J.*, 2019, **146**, 1218–1226.

8 B. K. Deka, T. K. Maji and M. Mandal, Study on properties of nanocomposites based on HDPE, LDPE, PP, PVC, wood and clay, *Polym. Bull.*, 2011, **67**(9), 1875–1892.

9 A. Awasthi, P. Jadhao and K. Kumari, Clay nano-adsorbent: structures, applications and mechanism for water treatment, *SN Appl. Sci.*, 2019, **1**, 1076.

10 A. Scala, A. Piperno, A. Hada, S. Astilean, A. Vulpoi, G. Ginestra, *et al.*, Marine bacterial exopolymers-mediated green synthesis of noble metal nanoparticles with antimicrobial properties, *Polymers*, 2019, **11**(7), 1157.

11 J. Madejová, FTIR techniques in clay mineral studies, *Vib. Spectrosc.*, 2003, **31**, 1–10.

12 M. M. Hassan, M. Zareef, T. Jiao, S. Liu, Y. Xu, A. Viswadevarayalu, *et al.*, Signal optimized rough silver nanoparticle for rapid SERS sensing of pesticide residues in tea, *Food Chem.*, 2021, **338**, 127796–127803.

13 X. Zhao, N. Li, M. Jing, Y. Zhang, W. Wang, L. Liu, *et al.*, Monodispersed and spherical silver nanoparticles/graphene nanocomposites from gamma-ray assisted in situ synthesis for nitrite electrochemical sensing, *Electrochim. Acta*, 2019, **295**, 434–443.

14 M. Frezza, S. Hindo, D. Chen, A. Davenport, S. Schmitt, D. Tomco, *et al.*, Novel metals and metal complexes as platforms for cancer therapy, *Curr. Pharm. Des.*, 2010, **16**(16), 1813–1825.

15 Z. S. Pillai and P. V. Kamat, What factors control the size and shape of silver nanoparticles in the citrate ion reduction method?, *J. Phys. Chem. B*, 2004, **108**(3), 945–951.

16 D. A. C. Brownson and C. E. Banks, Interpreting Electrochemistry, in *The Handbook of Graphene Electrochemistry*, Springer London, 2014, pp. 23–77.

17 J. Chen, J. Shao, R. Cai, Y. Shen, R. Zhang, L. Liu, *et al.*, Anti-retroviral therapy decreases but does not normalize indoleamine 2,3-dioxygenase activity in HIV-infected patients, *PLoS One*, 2014, **9**(7), 3–10.

18 N. Aristov and A. Habekost, Cyclic Voltammetry-A Versatile Electrochemical Method Investigating Electron Transfer Processes, *World J. Chem. Educ.*, 2015, **3**(5), 115–119.

19 N. Elgrishi, K. J. Rountree, B. D. McCarthy, E. S. Rountree, T. T. Eisenhart and J. L. Dempsey, A Practical Beginner's Guide to Cyclic Voltammetry, *J. Chem. Educ.*, 2018, **95**(2), 197–206.

20 J. Rupar, M. M. Aleksić, K. Nikolić and M. R. Popović-Nikolić, Comparative electrochemical studies of kinetic and thermodynamic parameters of quinoxaline and brimonidine redox process, *Electrochim. Acta*, 2018, **271**, 220–231.

21 S. Y. Vassiliev, V. V. Sentyurin, E. E. Levin and V. A. Nikitina, Diagnostics of lithium-ion intercalation rate-determining step: distinguishing between slow desolvation and slow charge transfer, *Electrochim. Acta*, 2019, **302**, 316–326.